electronics

MDPI

Article

A Non-Contact Integrated Body-Ambient Temperature Sensors Platform to Contrast COVID-19

Sandra Costanzo [1,2,3,4,*] and Alexandra Flores [1]

1 Dipartimento di Ingegneria Informatica, Modellistica, Elettronica e Sistemistica, Università della Calabria, 87036 Rende, Italy; flrlnd93d56z605o@studenti.unical.it
2 ICEmB (Inter-University National Research Center on Interactions between Electromagnetic Fields and Biosystems), 16145 Genoa, Italy
3 National Research Council of Italy (CNR), Institute for Electromagnetic Sensing of the Environment (IREA), 80124 Naples, Italy
4 CNIT (Consorzio Nazionale Interuniversitario per le Telecomunicazioni), 43124 Parma, Italy
* Correspondence: costanzo@dimes.unical.it; Tel.: +39-0984-494652

Received: 5 September 2020; Accepted: 3 October 2020; Published: 12 October 2020

check for updates

Abstract: An integrated sensors platform for non-contact temperature monitoring is proposed in this work. The adopted solution, based on the combined integration of an infrared thermometer and a capacitive humidity sensor, is able to provide a fast and accurate tool for remotely sensing both ambient and body temperature in the framework of pandemic situations, such as COVID-19, thus avoiding any direct contact with people. The information relative to the ambient temperature is successfully exploited to derive a correction formula for the accurate extraction of body temperature from the measurement provided by the standard infrared sensor. Full details on the design of the proposed platform are provided in the work, by reporting relevant simulation results on the variations of ambient temperature, relative humidity, and body temperature. Experimental validations are also discussed to provide a full assessment of the proposed approach.

Keywords: COVID-19; infrared; thermometer; non-contact sensor; capacitive sensor

1. Introduction

Fever is one of the most important symptoms [1] of COVID-19, but due to the contagious effect, its measurement can become a serious problem, so it is important to perform the temperature detection of patients very quickly and possibly without any contact. On the other hand, both epidemiological and laboratory studies have revealed that ambient temperature could affect the survival and spread of Coronavirus [2], so that a continuous monitoring of temperature, regarding both ambient and body temperature, is an essential task to be performed in the contrast of COVID-19. The adoption of thermographic systems in the framework of pandemic situations, such as COVID-19, can be decisive for initial temperature assessment devoted to medical purposes, namely:

- Initial human temperature screening during the triage process in a public health emergency, to determine the significance of fever and elevated temperature with respect to possible affection;
- Temperature assessment within high throughput areas, such as business structures, airports, etc.

The additional monitoring of ambient temperature can be strongly helpful to improve the accuracy in the detection of human body temperature, the measurement of which can be affected by the environmental humidity. Furthermore, recent studies have confirmed the effects of environmental temperature and humidity values in the increased risk of COVID-19 transmission [3].

A variety of solutions exist in terms of advanced sensor monitoring, but separately working for ambient humidity or human body temperature sensing, through the adoption of wireless IoT platforms in the first case [4] or wearable sensors for automated temperature monitoring of the patients [5] in the second case. Larger research has been mainly focused on the adoption of sophisticated solutions for fever monitoring and contact tracing [6–8]. An extensive review of non-contact temperature assessment devices, with specific reference to the COVID-19 pandemic, can be found in [9], while interesting studies on the accuracy assessment for infrared imaging tools under specific conditions can be found in [10] and references herein. More advanced results have been recently presented, which are addressed to the detection of abnormal breathing signals [11]. All the above solutions require a cost that is not easily accessible for massive adoption; moreover, they do not include the detection of environmental parameters, such as humidity, which can give useful information for tracing the pandemic disease.

To the authors' knowledge, no integrated platform exists to simultaneously perform a non-contact sensing of both ambient and body temperatures. Such a platform could be very helpful to accurately perform both the monitoring of infected people (body temperature capturing) and the control of pandemic spreading, which can be affected by ambient conditions, such as relative humidity [2]. If joined with heart rate variability (HRV) information, body temperature monitoring can also be helpful to predict COVID-19 infection before symptoms appear, thus leading to early detection technology.

To this end, an integrated hardware system is proposed in the present work, which includes two typologies of sensors able to separately capture ambient and human body temperature [5,12] values, with no overlap between them. As compared with solutions existing in the market that are typically able to perform a remote body temperature detection, a compact and low-cost platform solution (estimated max cost: roughly 10 euros) is proposed to capture both the body and ambient temperature, thus being strongly helpful for the investigation of the potential association of climate and seasonality with the spread of the infection, in the framework of preventive and surveillance strategies [13]. Two different sensors are specifically adopted to realize the above task, namely, an infrared temperature sensor [14] and a relative humidity (RH) level sensor [12], which are integrated to provide a unique measurement system for the temperature parameters, easily displayed on a LED screen. Studies regarding the influence of ambient parameters on the spreading of COVID-19 are in progress, and no consolidated theory exists regarding this. Thus, the inclusion of ambient humidity can be helpful for providing additional information data towards the establishment of an ever-improved specific theory to well-characterize COVID-19 and to distinguish it from other similar pandemics. The combined thermometer prototype can be easily adopted as a remote sensing device in all situations requiring fast and accurate temperature monitoring to prevent and control COVID-19 spreading. For example, it can be directly mounted in a patient's room, with no required action from health workers and with the possibility to remotely control the temperature values by the medical staff.

The paper is organized as follows. In Section 2, the architecture of the proposed multi-sensor platform is described, with all details relative to the reconstruction formulas for relative humidity, ambient temperature, and body temperature. Simulation results are fully reported in Section 3, by successfully comparing reconstruction and ideal data, thus demonstrating the high accuracy of the proposed approach. In Section 4, experimental validations are discussed, and the relevant correction formula is presented to accurately extract the body temperature from the ambient and body temperature measurements provided by the proposed platform. Conclusions are finally outlined in Section 5.

2. A Non-Contact Sensors Platform for Remote Ambient-Body Temperature Monitoring

The architecture of the proposed sensors platform is illustrated in Figure 1. In particular, the section corresponding to the infrared sensor, for the measurement of body temperature, consists of a lens that is able to filter the infrared radiation emitted by the examined body and concentrate it on a photoresist temperature sensor. This performs the conversion into a current signal, which, in turn, is transformed into the relative temperature value, configured on the Arduino microcontroller. The second section of the platform corresponds to the capacitive relative humidity (RH) sensor, which is conditioned to obtain a voltage value at the output. This is entered into the microcontroller, to be manipulated and to finally obtain the RH and ambient temperature value to be displayed, together with the body temperature on an LED display. The proposed architecture, whose main novelty is the low-cost integration and control of two different sensors, includes a single platform with two distinct features, namely, the ability to separately control human body temperature and environmental parameters, such as relative humidity and ambient temperature. These two capabilities can be adopted together, as well as in a separate way, depending on the specific purpose (fever detection, ambient temperature check, and control, etc.). Moreover, the introduced additional information relative to the ambient temperature can be successfully adopted to compensate for the error due to the emissivity related to the surrounding environment, which is not directly taken into account by a standard infrared thermometer.

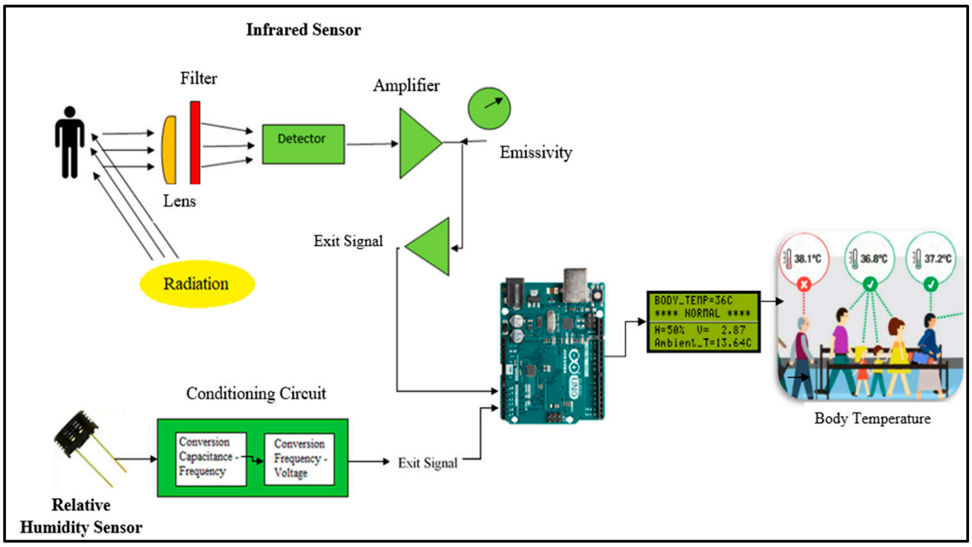

Figure 1. Proposed sensors platform for remote ambient and body Temperature monitoring.

2.1. Relative Humidity Computation

Capacitance is an electrical property existing between two conductors, which are separated by a non-conductor material. The simplest model is given by two metal plates with an air space separation. It is well known that the above parameter is influenced by the three factors, namely [15]:

$$C = \frac{A\varepsilon}{d} \tag{1}$$

where:

A = the area of the plates;
d = the distance between the two conductors;
ε = the electrical permittivity of the non-conductor material.

Capacitive sensors are a type of electrical sensor that react to changes in the capacitance. Therefore, they can be used to measure any parameter that, if varied, produces a relative change in the capacitor parameter. Such variation will cause a change in the currents and the voltages of the circuit, including the capacitor, thus affecting the humidity.

To realize the RH sensing from capacitance variations, a conditioning method recommended by standard manufacturers [16] was adopted, the circuit for which is illustrated in Figure 2.

The humidity sensor, assumed as a reference, is that belonging to the HS1101LF family [12], and has the following characteristics:

- Maximum supply voltage equal to 10 V;
- Unrestricted frequency range between 5 kHz and 300 kHz;

- Ability to measure between 0% (RH) and 100% (RH), which correspond, respectively, to the minimum (161.6 pF) and maximum (193.1 pF) capacitance values.

There are several ways to convert a sensor's capacitance value to a voltage value, but oscillator-based methods are generally used to condition capacitive RH sensors. The basic idea of this type of conditioner is to perform a two-step conversion, as shown in Figure 2.

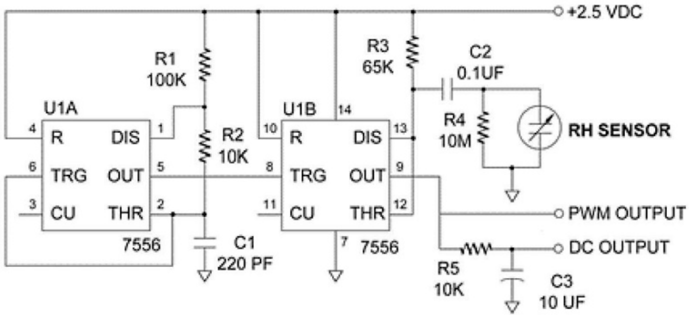

Figure 2. Recommended signal conditioner circuit for capacitive sensors [16].

1. First Step: Capacity-Frequency Conversion (CFC)

The process of charging and discharging a capacitor can be used to generate a periodic signal, whose frequency is related to the time constant of the capacitor. In this way, changes in sensor capability will result in signal frequency variations. Square wave oscillators are generally adopted, such as the 555 based multivibrator [16]. The circuit generated a periodic signal with a stable multivibrator, which acted as a trigger signal for a monostable. This therefore generated an impulse, whose duration was proportional to the sensor capacity, finally obtaining a square signal with a duty cycle proportional to the capacity value, namely a pulse width modulation (PWM) signal.

2. Second Step: Frequency-Voltage Conversion (FVC)

In this second phase, the PWM signal was filtered, thus obtaining its DC component, whose value was proportional to the capacity and, therefore, to the relative humidity. The above voltage value was entered into the microcontroller for its manipulation and thus to obtain the humidity level.

The structural scheme for the conditioning of the capacitive sensor is illustrated in Figure 3. Starting with the stable stage, it followed the monostable stage (where the capacitive sensor was connected), having the function to vary the capacitance in a range between 161.6 pF and 193.1 pF. After that, signal filtering (PWM) was performed, and the achieved value was configured in the microcontroller to finally obtain a relative humidity value to be displayed at the user.

A detailed description of the various blocks included in the structural frame is reported in the following.

Stable Stage:

Set a frequency of 10 KHz and a duty cycle of 90% and solve using the equations provided by the datasheet [12]:

$$f = \frac{1.44}{(RA + 2RB)C} \tag{2}$$

$$= \frac{RA + RB}{RA + 2RB}, \tag{3}$$

where:

f = the frequency (Hz);
D = the duty cycle (%);
RA, RB = the resistors (Ω);

C = the capacitor (F).

From the above procedure, the following commercial values are obtained: RA = 115 kΩ, RB = 14.3 kΩ, and C = 1 nΩ.

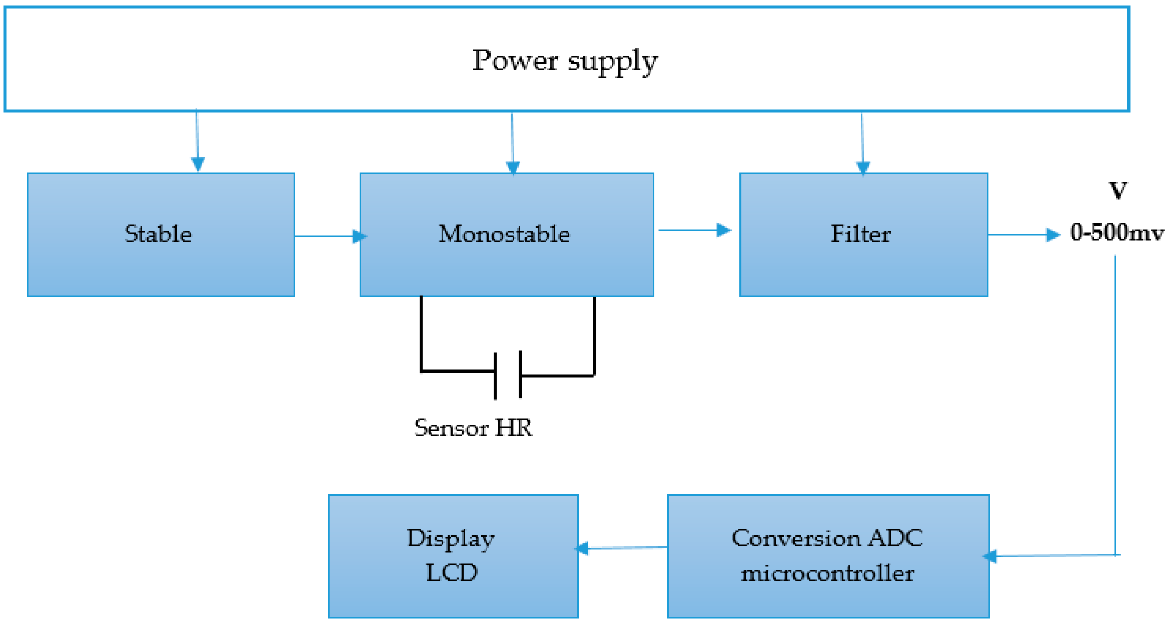

Figure 3. Structural scheme for the conditioning of the capacitive sensor.

Monostable Stage:

Following the equation provided in the datasheet [12], by taking into account that the output signal is a PWM signal, with time t, given by:

$$\mathrm{t} = -\ln\left(\frac{1}{3}\right) \times RCs = 1.1 \times R\,Cs, \tag{4}$$

where:

t = time (s);
R = the resistor (Ω);
Cs = the variable capacitor of the HS1101LF sensor (F).

From Equation (4), by fixing:

$$R = 320.666\ \text{k}\Omega, \tag{5}$$

We have

$$t_1 = 1.1 \times (320.666\ \text{k}\Omega) \times (161.6\ \text{pF}) = 5.7 \times 10^{-5}\ \text{s}, \tag{6}$$

$$t_2 = 1.1 \times (320.666\ \text{k}\Omega) \times (170.7\ \text{pF}) = 6.02 \times 10^{-5}\ \text{s}, \tag{7}$$

$$t_3 = 1.1 \times (320.666\ \text{k}\Omega) \times (178.5\ \text{pF}) = 6.29 \times 10^{-5}\ \text{s}, \tag{8}$$

$$t_4 = 1.1 \times (320.666\ \text{k}\Omega) \times (185.7\ \text{pF}) = 6.55 \times 10^{-5}\ \text{s}, \tag{9}$$

$$t_5 = 1.1 \times (320.666\ \text{k}\Omega) \times (193.1\ \text{pF}) = 6.81 \times 10^{-5}\ \text{s}, \tag{10}$$

In addition, we can compute:

$$Vout(t_i) = Vcc \times \frac{t_i}{T} = Vcc \times \frac{t_i}{\frac{1}{f}}, \tag{11}$$

where:

$Vout$ = the output voltage (V);
Vcc = 4.5, the supply voltage (V);
Δt = time (s);
f = the frequency (Hz).

From the above expression, we can obtain the ideal values for the output voltages, namely:

$$V_{out(0\%RH)} = 2.565 \text{ V}, \tag{12}$$

$$V_{out(25\%RH)} = 2.710 \text{ V}, \tag{13}$$

$$V_{out(50\%RH)} = 2.833 \text{ V}, \tag{14}$$

$$V_{out(75\%RH)} = 2.948 \text{ V}, \tag{15}$$

$$V_{out(100\%RH)} = 3.065 \text{ V}, \tag{16}$$

In addition, the manufacturer specified that the HS1101LF humidity sensor cannot be fed with direct current, therefore the sensor was positioned in the present design after an RC high pass filter with a very high R value and a very low C value.

Filter Stage:

The final signal of the circuit must be a continuous signal. To this end, we resorted to filter the PWM signal through a low pass filter, and then we eliminated the alternating component. A cutoff frequency equal to 2 Hz was fixed for the filter.

In Figure 4, the simulation scheme implemented on Proteus Software is reported, which includes all steps to be followed for the conditioning procedure of the capacitive sensor, to have a voltage value for proper manipulation of the Atmega328p microcontroller and final reconstruction of the relative humidity level.

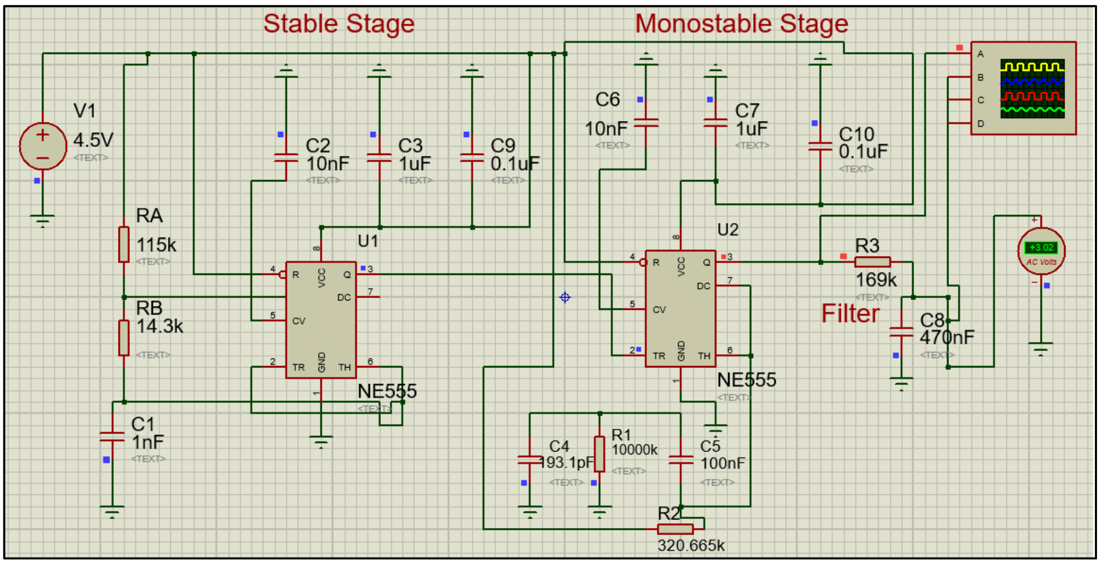

Figure 4. Proteus simulation scheme for the reconstruction of the relative humidity level.

Table 1 shows the results in terms of voltage values obtained from simulation for each capacitance value. The comparison with the ideal values computed using Equations (12)–(16) reveals very good accuracy in the proposed approach.

Table 1. Voltage value, ideal and simulated.

RH%	C(pf)	Vout (V) Ideal	Vout (V) Simulation
0	161.6	2.565	2.6
25	170.7	2.710	2.74
50	178.5	2.833	2.87
75	185.7	2.948	2.98
100	193.1	3.065	3.10

From data reported in Table 1, the equation describing the sensor behavior, in terms of humidity value correlation vs. voltage, is obtained, and the relative curve is represented in Figure 5.

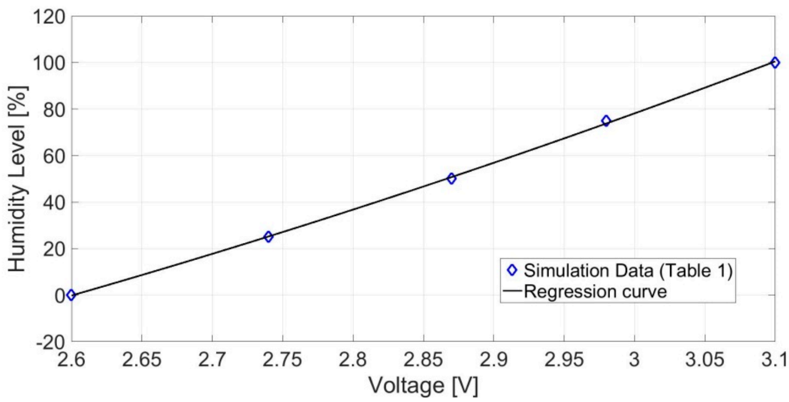

Figure 5. Humidity value correlation vs. sensor voltage.

In particular, the following regression formula is obtained to describe the sensor response:

$$y = p_1 \times x^2 + p_2 \times x + p_3, \tag{17}$$

where:

y = the relative humidity (%);
x = the voltage (V);
p_1 = 55.43;
p_2 = −114.6;
p_3 = −76.87.

The above equation was subsequently implemented on the microcontroller to realize the processing and visualization of the relative humidity level.

2.2. Ambient Temperature Computation

To retrieve the ambient temperature value from the relative humidity level, a psychometric chart [17] was adopted (Figure 6). The relative humidity is the percentage of saturation of a specific volume of air at a specific temperature. The relative humidity of the air depends on the temperature and pressure of the analyzed air volume, which can also be expressed in terms of absolute humidity (grams of water per unit volume). The temperature at which the moisture content in air reaches its saturation point occurs at 32 °F or 0 °C. At a humid air bulb temperature of 0 °C, we have 4.9 gm/m^3 of absolute humidity. Then, from this absolute humidity value and the relative humidity values, the actual temperature value can be obtained.

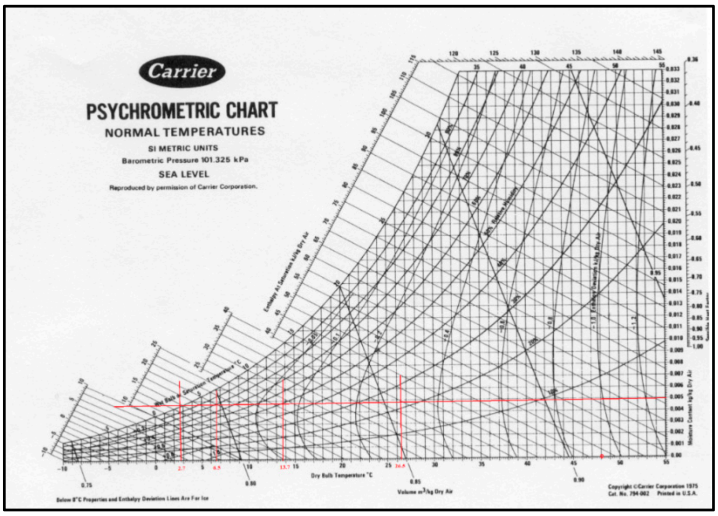

Figure 6. Psychometric chart for the temperature evaluation.

The results of the above computations are summarized in Table 2.

Table 2. Relative humidity and temperature obtained from the psychrometric chart.

Relativity Humidity (%)	Dry Bulb Temperature (°C)
0	48
25	26.5
50	13.7
75	6.5
100	2.7

The equation relating the temperature values to the corresponding relative humidity levels is derived from data reported in Table 2. It is properly represented in Figure 7.

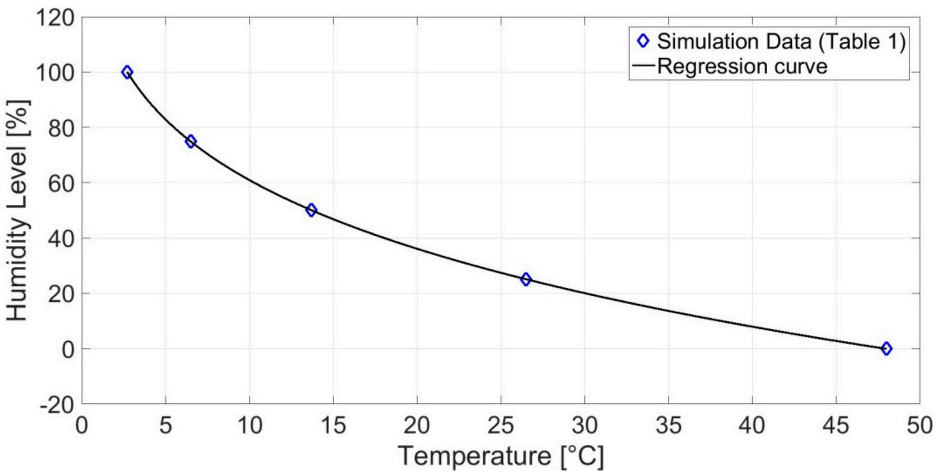

Figure 7. Temperature value correlation vs. relative humidity.

The corresponding equation is given as:

$$y = a \times x^b + c, \tag{18}$$

where:

y = the relative humidity (%);

x = the temperature °C;
a = −121.3;
b = 0.18;
c = 245.5.

The temperature unknown x is finally obtained by inverting Equation (18) to have:

$$x = 10^{\frac{log(\frac{y-c}{a})}{b}} \tag{19}$$

Equation (19) should be implemented on the microcontroller for the relative visualization of both relative humidity and ambient temperature results.

2.3. Body Temperature Computation

According to Stefan–Boltzmann's law, the temperature of an object can be estimated from the knowledge of its emissive power. Although radiation can occur over a wide range of wavelengths, the peak value of the most commonly desired temperature ranges is in the area of the spectrum corresponding to the infrared radiation [18]. In infrared thermography [19,20], this feature is used for multiple purposes, namely, as a health indicator in medical applications or as a fault detection in mechanical or electrical maintenance. Among the existing non-contact body temperature sensors, one of the most popular is that belonging to the MLX90614 family; an infrared thermometer that has a small size, low cost, and high accuracy [14]. MLX90614 is a non-contact infrared temperature sensor manufactured by the Melexis company. It can be easily connected to a processor, such as Arduino, for measuring the temperature of an object at a distance. Due to its low noise amplifier, 17-bit ADC, and powerful digital signal processor (DSP) unit, a thermometer with high accuracy and resolution can be achieved. The thermometer comes factory calibrated with a digital PWM and System Management Bus (SMBus) output. As a standard, the 10-bit PWM is configured to continuously transmit the measured temperature in a range between −20 °C and 120 °C, with an output resolution of 0.14 °C, and the POR default is SMBus, with a resolution of 0.02 °C [18]. The microcontrollers have an I^2C communication way to connect with external peripherals; the MLX 90614 thermometer also includes I^2C communication lines to be able to connect this sensor with the microcontroller, without any additional circuit (Figure 8). The sensor operates with a 3.3 V DC supply. If the micro controller operates with a 5 V DC, then it is necessary to pull up resistors between SDA and SCL lines to the +3.3 V DC line.

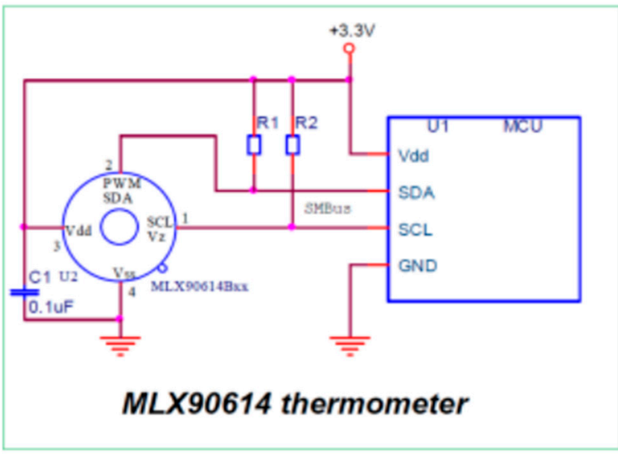

Figure 8. MLX90614 connection to System Management Bus (SMBus).

In Figure 9, the internal configuration of the MLX90614 sensor is reported. It is made up of a silicon chip with a fine micromechanized membrane that is sensitive to infrared radiation, together with the necessary hardware to amplify and digitize the signal and then compute the temperature. The set includes a low noise amplifier, a 17-bit ADC converter, a digital signal processor (DSP), and an ambient temperature compensation.

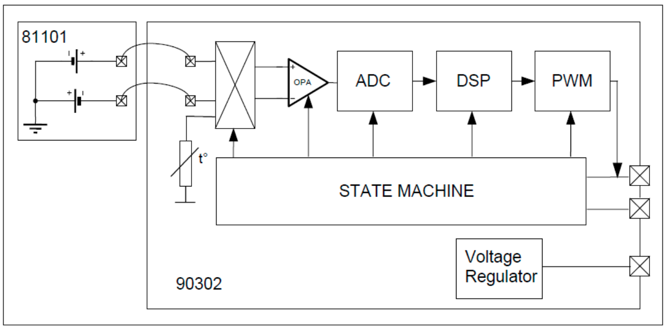

Figure 9. Block Diagram of the MLX90614 sensor.

In Figure 10, the graph of the field of view (FOV) [21], relative to the MLX90614 sensor, is reported, which is approximately equal to 35°. It is determined when a thermopile receives 50% of the radiation signal, and it is also related to the main axis of the sensor. Measurement accuracy is only guaranteed when the test object fully covers the field of view of the infrared sensor.

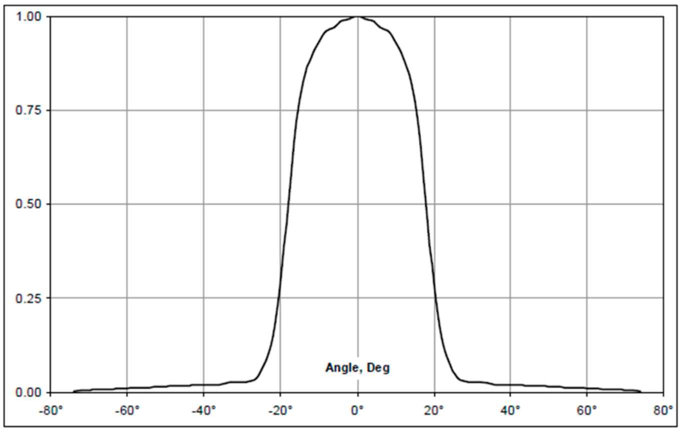

Figure 10. Field of view (FOV) graph relative to the MLX90614 sensor [21].

The following expression applies:

$$\tan(\text{FOV}) = \frac{\text{radius of test object}}{\text{distance between infrared sensor and test object}} \tag{20}$$

For example, if the radius of the test object is equal to 5 cm, then the measurement distance must be equal to 7 cm to achieve an accurate result.

In Figure 11, the steps for the configuration and programming of the MLX90614 temperature sensor on Arduino software are reported. In particular, a normal value is assumed if the measured temperature is in a range between 35 °C and 38 °C; for a temperature value greater than 38 °C, an alarm (LED) should light up, while for measured values lower than 35 °C, the temperature is assumed to be low. These results are displayed on the LED screen to be viewed by the user.

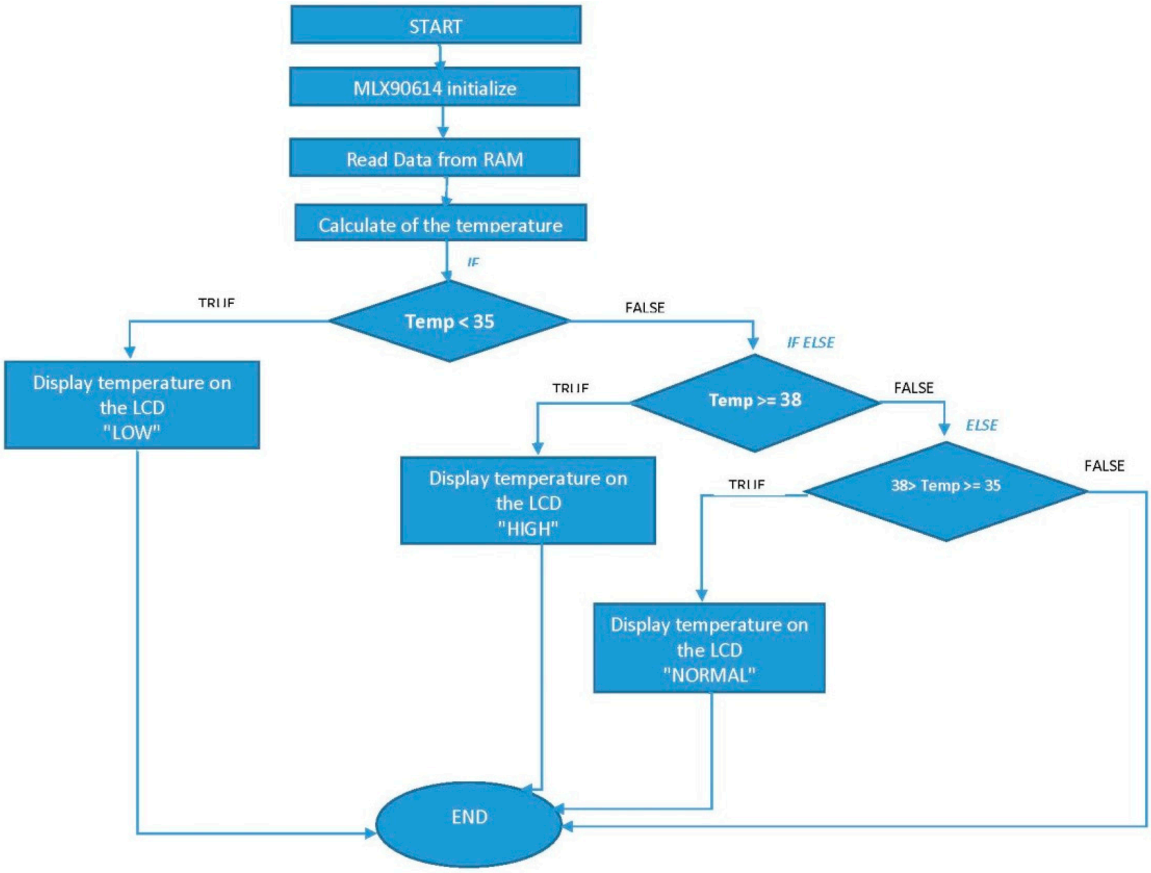

Figure 11. Schematic of the algorithm for the MLX90614 sensor.

Arduino boards have I^{2}C communication lines, which are easy to connect to I^{2}C by cable. The sensor must be connected as indicated in Figure 12. In order to provide a +3.3 V power supply from the Arduino board to the sensor, 4.7 KΩ resistors are used to realize pull up on the I^{2}C lines [22].

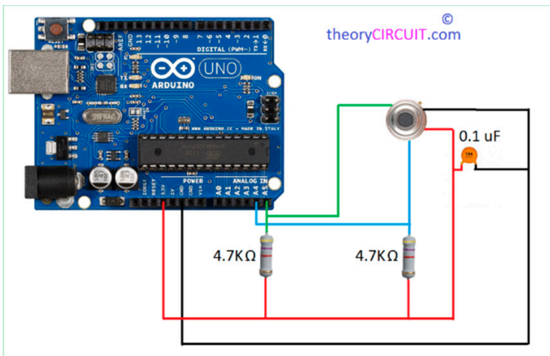

Figure 12. Arduino connection diagram for the MLX90614 sensor [22].

3. Simulation Results

The relative humidity sensor, the ambient temperature, and the infrared temperature sensor were integrated into a single system, as shown in Figures 13 and 14. Software development was carried out on the Arduino uno ATmega328p microcontroller. The two sensors were controlled independently to avoid inaccuracies, but their measurements were performed at the same time, and the acquired values were shown in a few seconds sequence. In addition, an alarm was incorporated, so that LED would light up if the body temperature was greater than 38 °C.

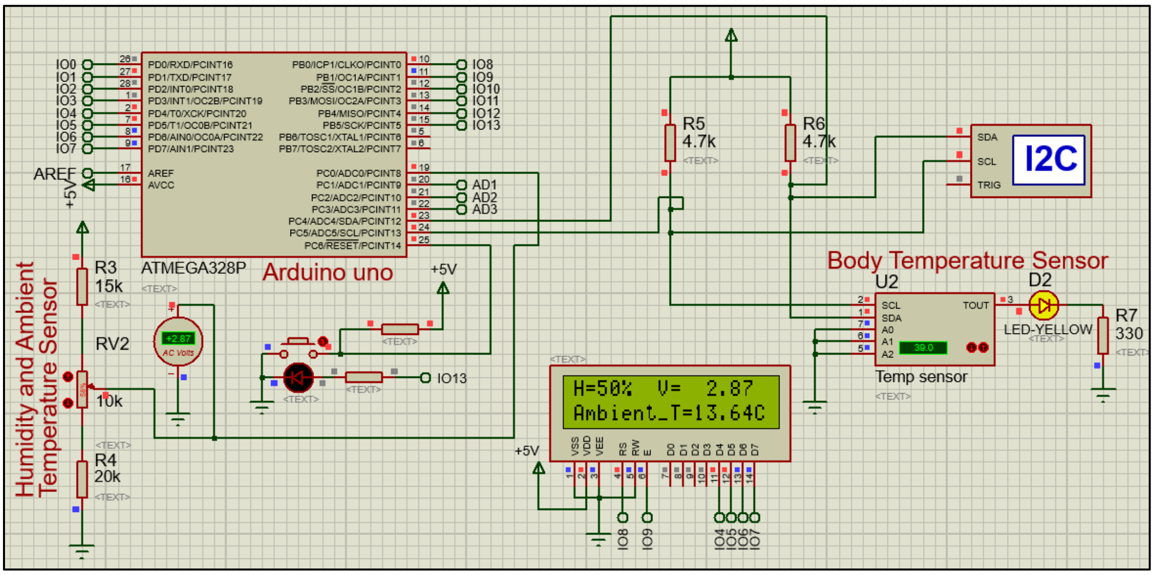

Figure 13. Final simulation of the prototype: Visualization of the relative humidity and ambient temperature.

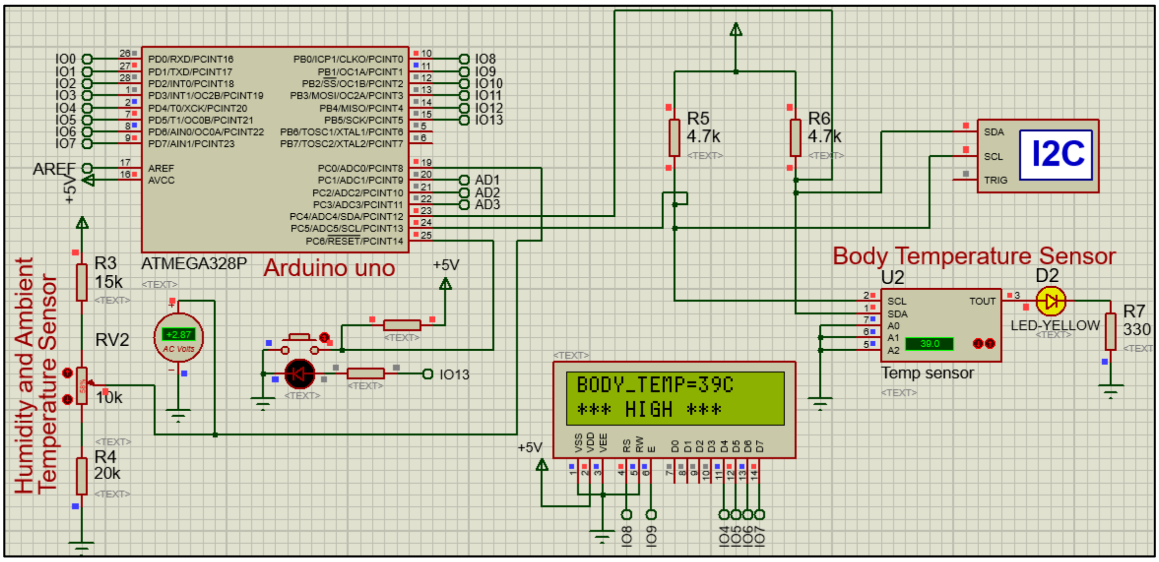

Figure 14. Final simulation of the prototype: Visualization of body temperature.

The results obtained from simulations, corresponding to each sensor, are reported in Tables 3 and 4, respectively.

Table 3. Simulation results for relative humidity (RH) and ambient temperature.

C(pf)	Ideal RH%	Simulated RH%	Ideal Vout (V)	Simulated Vout (V)	Ideal Temperature (°C)	Simulated Temperature (°C)
161.6	0	0	2.565	2.6	48	48.03
170.7	25	26	2.710	2.74	26.5	25.83
178.5	50	50	2.833	2.87	13.7	13.64
185.7	75	73	2.948	2.98	6.5	6.86
193.1	100	100	3.065	3.10	2.7	2.71

Table 4. Simulation results for body temperature and power radiation values at different emissivity values.

Simulated body Temperature (°C)	State	Body Temperature (°K)	Emissivity ϵ	Power Radiation W/m^2
30	LOW	303.15	-	95.71
34	LOW	307.15	-	100.9
36	NORMAL	309.15	0.2	103.5
38	HIGH	311.15	-	106.2
40	HIGH	313.15	-	109.1
30	LOW	303.15	-	287.2
34	LOW	307.15	-	302.5
36	NORMAL	309.15	0.6	310.5
38	HIGH	311.15	-	318.7
40	HIGH	313.15	-	327.1
30	LOW	303.15	-	478.5
34	LOW	307.15	-	504.3
36	NORMAL	309.15	1.0	517.4
38	HIGH	311.15	-	531.3
40	HIGH	313.15	-	545.3

In Figure 15, the comparison between humidity values obtained from simulated and ideal voltages is illustrated by revealing a linearity in response with 95% confidence.

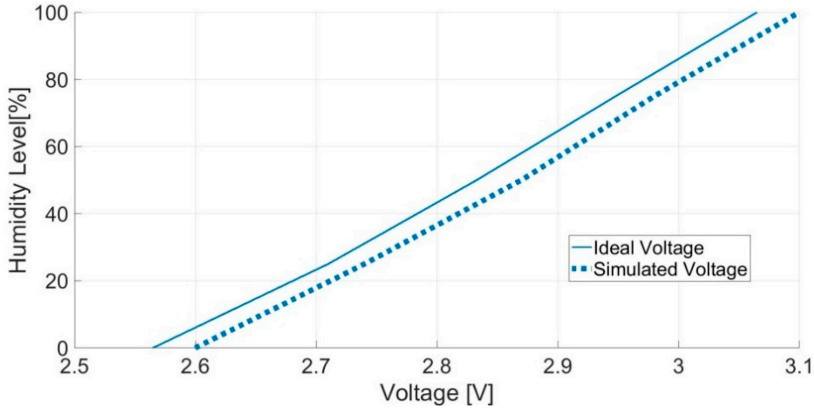

Figure 15. Comparison between humidity values obtained from simulated and ideal voltages.

In Figure 16, the humidity curves obtained from ideal and simulated temperature values are reported, and a negligible variation can be observed.

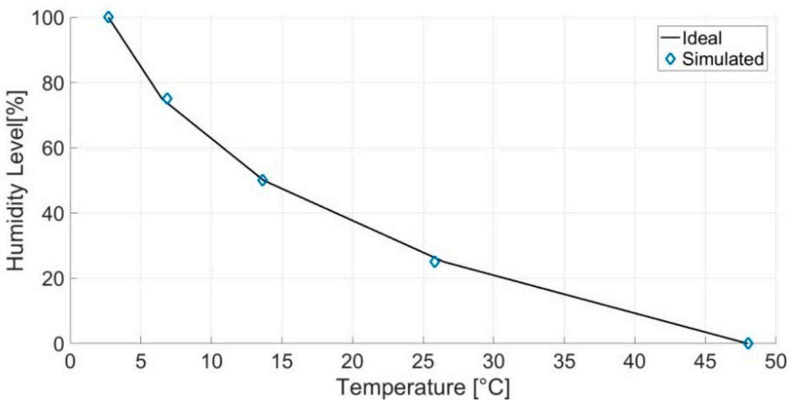

Figure 16. Comparison between humidity values obtained from simulated and ideal temperature.

As previously outlined, the body temperature T can be retrieved from the emissivity value by inverting the Stefan–Boltzmann's law to have:

$$T = (\frac{W}{\epsilon \times \sigma})^{1/4} \tag{21}$$

The corresponding graph, for various emissivity values (in the typical range for a human body), is illustrated in Figure 17.

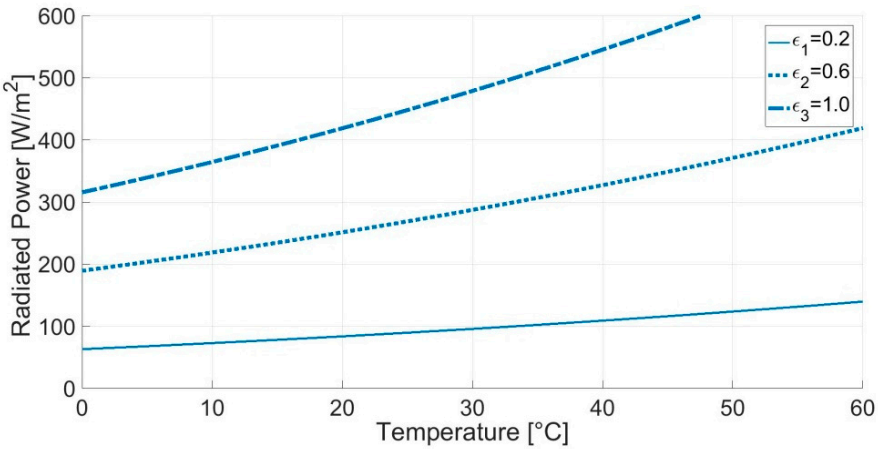

Figure 17. Body temperature vs. radiated power for various emissivity values.

4. Experimental Results

To fully validate the proposed multisensor platform, in terms of the enhanced correction algorithm for the accurate detection of body temperature, a prototype was realized into the Microwave Laboratory at the University of Calabria and various sets of measurements were performed.

As a first step, to demonstrate the accuracy improvement in the infrared measurements obtained from the adoption of ambient humidity and temperature, human body temperature data acquired with the proposed platform were compared, with the values measured through a standard reference thermometer. Measurements were repeated for different values of ambient temperature and relative humidity, obtaining average errors (difference between infrared and standard thermometer values) in the range 3–7. An example of the dataset extracted from the above set is reported in Table 5.

Table 5. Measurement results: Comparison between infrared and traditional thermometer values of body temperature before calibration with ambient parameters.

Implemented System			Traditional Thermometer	Body Temperature Difference
Ambient Temperature (°C)	**Relative Humidity (%)**	**Body Temperature (°C)**	-	-
29	67	31.11	36.6	5.49
29	67	31.1	36.5	5.4
29	67	31.13	36.4	5.27
29	67	31.13	36.7	5.27
29	67	31.12	36.3	5.18
Average		31.12	36.5	5.32

Data obtained from the above measurement campaign were applied to realize the accurate calibration of the MLX90614 sensor, thus achieving a temperature compensation that ensures extremely accurate results. The following polynomial correction formula was extracted from the above data, which was able to provide the true body temperature by exploiting the information relative to the ambient temperature:

$$T_b = a_1 + a_2 T_S + a_3 T_a + a_4 {T_S}^2 + a_5 T_S T_a + a_6 {T_a}^2 \tag{22}$$

Parameters appearing in Equation (22) have the following meaning:

T_b = the correct body temperature;
T_S = the measured system temperature;
T_a = the ambient temperature.

Correction coefficients have the following values: $a_1 = 9.25$, $a_2 = 4.08$, $a_3 = -2.65$, $a_4 = -0.16$, $a_5 = 0.2$, $a_6 = -0.06$.

In Figure 18, the graph representation of the curve given by Equation (22) is provided, where the proper match of the standard thermometer measurements with the proposed fitting mesh can be observed.

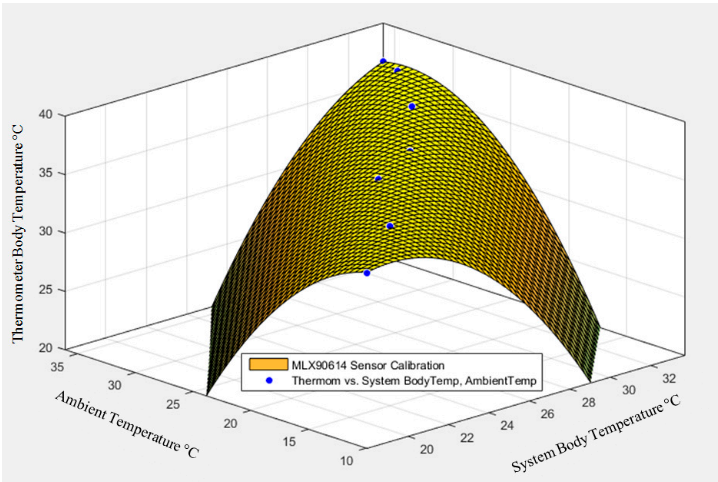

Figure 18. Fitting curve representation for accurate body temperature extraction.

After the above calibration step, body temperature measurements were performed on a human subject (Figure 19) to provide the final assessment of the proposed approach. An optimum measurement distance equal to 10 cm was verified and applied. A measurement time equal to 1 s was required.

Figure 19. Proposed multisensor platform adopted to perform accurate body temperature measurements.

Body temperature data captured at different times in a day are summarized in Table 6, where the comparison with measurements performed through a traditional thermometer are also reported.

Each measurement was repeated five times, and the average data are reported in Table 6. A very small average error (0.47%) can be successfully observed.

Table 6. Measurement results: Comparison between infrared and traditional thermometer values of body temperature after calibration with ambient parameters.

Hour	Implemented System			Traditional Thermometer	Absolute Error	Relative Error %
-	Body temperature (°C)	Ambient temperature (°C)	Relative humidity (%)	-	-	-
6:00	35.85	24	70	35.9	0.05	0.14
10:00	36.21	29	54	36.4	0.19	0.52
14:00	36.75	34	52	36.9	0.15	0.41
16:00	36.51	31	57	36.7	0.19	0.52
17:00	36.32	29	59	36.6	0.28	0.76
21:00	36.12	28	63	36.3	0.18	0.49
Average error						0.47

5. Conclusions

An integrated platform combining multiple sensors for the simultaneous non-contact measurement of relative humidity, ambient temperature, and body temperature has been presented in this work. The operating principle and the full hardware design has been accurately described. Numerical simulations, reporting the curves for the three assumed variable parameters are shown and discussed to provide evidence of the nominal design. Experimental validations have also been provided to demonstrate the improved accuracy of infrared temperature measurements achieved with the proposed approach. This is particularly useful for detecting fevers and therefore possible infections of COVID-19 and other illnesses.

Author Contributions: The individual contributions of authors are specified as follows: Conceptualization, S.C.; Methodology, S.C.; Software, A.F.; Validation, S.C. and A.F.; Writing—Original draft preparation, S.C. and A.F.; Writing—Review and editing, S.C.; Supervision, S.C. All authors have read and agreed to the published version of the manuscript.

Funding: This research received no external funding.

Conflicts of Interest: The authors declare no conflict of interest.

References

1. Di Gennaro, F.; Pizzol, D.; Marotta, C.; Antunes, M.; Racalbuto, V.; Veronese, N.; Smith, L. Coronavirus Diseases (COVID-19) Current Status and Future Perspectives: A Narrative Review. *Int. J. Environ. Res. Public Health* **2020**, *17*, 2690. [CrossRef] [PubMed]
2. Xie, J.; Zhu, Y. Association between ambient temperature and COVID-19 infection in 122 cities from China. *Sci. Total Environ.* **2020**, *724*, 1–5. [CrossRef] [PubMed]
3. Xu, H.; Yan, C.; Fu, Q.; Xiao, K.; Yu, Y.; Han, D.; Wang, W.; Cheng, J. Possible environmental effects on the spread of COVID-19 in China. *Sci. Total Environ.* **2020**, *731*, 1–7. [CrossRef] [PubMed]
4. RadiantWatch IoT Platform. Available online: https://radiantwatch.com/ (accessed on 5 September 2020).
5. The Fight Against Novel Coronavirus: Automated Temperature Monitoring for COVID-19 Patients. Available online: http://www.vivalnk.com/covid-19 (accessed on 5 September 2020).
6. Thermal Cameras Are Being Outfitted to Detect Fever and Conduct Contact Tracing for COVID-19. Available online: https://spectrum.ieee.org/news-from-around-ieee/the-institute/ieee-member-news/thermal-cameras-are-being-outfitted-to-detect-fever-and-conduct-contact-tracing-for-covid19 (accessed on 5 September 2020).
7. With Safety in Phase 3 of the COVID-19 Pandemic. Available online: https://www.wikifriend.net/smart-health-coronavirus-thermal-scanner.html (accessed on 5 September 2020).

8. This Temperature-Screening System for COVID-19 Can Check Up to 9 People at Once. Available online: https://spectrum.ieee.org/news-from-around-ieee/the-institute/ieee-member-news/this-temperaturescreening-system-for-covid19-can-check-up-to-9-people-at-once (accessed on 5 September 2020).
9. Non-Contact Temperature Assessment Devices during the COVID-19 Pandemic. Available online: https://www.fda.gov/medical-devices/coronavirus-covid-19-and-medical-devices/non-contact-temperature-assessment-devices-during-covid-19-pandemic (accessed on 5 September 2020).
10. Zheng, K.; Dong, R.; Wang, H.; Granick, S. Infrared assessment of human facial temperature in the presence and absence of common cosmetics. *medRxiv* **2020**. [CrossRef]
11. Zheng, J.; Menghan, H.; Zhongpai, G.; Fan, L.; Ranran, D.; Pan, Y.; Tang, W.; Guangtao, Z.; Yong, L. Detection of Respiratory Infections using RGB-infrared sensors on Portable Device. *IEEE Sens. J.* **2020**. [CrossRef]
12. Relative Humidity Sensor. HS1101LF Meets RoHS Regulations. Available online: https://www.alldatasheet.es/datasheet-pdf/pdf/241417/HUMIREL/HS1101LF.html (accessed on 5 September 2020).
13. Sajadi, M.M.; Habibzadeh, P.; Vintzileos, A.; Shokouhi, S.; Miralles-Wilhelm, F.; Amoroso, A. Temperature, Humidity, and Latitude Analysis to Estimate Potential Spread and Seasonality of Coronavirus Disease 2019 (COVID-19). *JAMA Netw.* **2020**, *3*, 1–11. [CrossRef] [PubMed]
14. Usamentiaga, R.; Venegas, P.; Guerediaga, J.; Vega, L.; Molleda, L.; Bulnes, F.G. Infrared Thermography for Temperature Measurement and Non-Destructive Testing. *Open Access Sens.* **2014**, *1*, 12308–12310. [CrossRef] [PubMed]
15. Wang, D. FDC1004: Basics of Capacitive Sensing and Applications. *Tex. Instrum.* **2014**, *1*, 2.
16. Zdankiewicz, E.M.; A Comparison of Relative Humidity Sensing Technologies. HIGOMETRIX Applications Note 2004-2, Volume 1, p. 3. Available online: https://docplayer.net/22214027-A-comparison-of-relative-humidity-sensing-technologies.html (accessed on 5 September 2020).
17. Bhattacharya, Y.; Milne, M. *Psychrometric Chart Tutorial: A Tool for Understanding Human Thermal Comfort Conditions*; University of California: Los Angeles, CA, USA, 2009.
18. Giddings, S.B. Hawking radiation, the Stefan–Boltzmann law, and unitarization. *Phys. Lett. B* **2016**, *1*, 40–42. [CrossRef]
19. Lahiri, B.B.; Bagavathiappan, S.; Jayakumar, T.; Philip, J. Medical applications of infrared thermography: A review. *Infrared Phys. Technol.* **2012**, *1*, 226. [CrossRef] [PubMed]
20. Karakostopulos, K. MLX90614 family Single and Dual Zone Infra Red Thermometer in TO-39. *Melexis Microelectron. Integr. Syst.* **2008**, *1*, 1–42.
21. IR Thermometer Sensor MLX90614 SKU: SEN0206. Available online: https://wiki.dfrobot.com/IR_Thermometer_Sensor_MLX90614_SKU__SEN0206 (accessed on 5 September 2020).
22. Infrared Thermometer Arduino. Available online: http://www.theorycircuit.com/infrared-thermometer-arduino/ (accessed on 5 September 2020).